J Electr Eng Technol.2018; 13(4): 1596-1603
http://doi.org/10.5370/JEET.2018.13.4.1596

ISSN(Print) 1975-0102
ISSN(Online) 2093-7423

Design of Linear Transverse Flux Machine for Stelzer Machine using Equivalent Magnet Circuit and FEM

Sung-In Jeong†

Abstract – This paper presents the new design and validation process of the linear transverse flux machine of the stelzer machine for hybrid vehicle application. A linear transverse flux machine is a novel electric machine that has higher force density and power than conventional electric machine.
The process concentrates on 2-dimensional and 3-dimensional analysis using equivalent magnetic circuit method considering leakage elements and it is verified by finite element analysis. Besides the force characteristics of all axis of each direction are analyzed.
The study is considered by dividing the transverse flux electric excited type and the transverse flux permanent magnet excited type. Additionally three-dimensional analysis in this machine is accomplished due to asymmetric structure with another three axes. Finally, it suggests the new design and validation process of linear transverse flux machine for stelzer machine.

Keywords: Equivalent magnetic circuit, Finite element analysis, Flux matrix, Force density, Free piston engine, Leakage element, Magnetic energy, Transverse flux electric, Transverse flux permanent magnet.

1. Introduction

Extensive use of fossil fuels such as gas, oil, and coal as an energy source leads to significant amounts of CO_2 and another pollutants being produced. Especially, an application of automotive industry is at risk to the people directly due to originated exhaust gases. Therefore, much study is being undertaken to develop more environmental friendly and advanced technology for the future. As a result, hybrid electric vehicles using the stelzer machine called the "Free Piston Engine" has a good solution to overcome these problems [1]. The stelzer machine is not commonly used to distinguish a linear machine from a rotating crankshaft machine. The meaning of piston is "Free" because it is motion in not restricted but unrestricted by piston of a rotating crankshaft as known from conventional engines. For this reason, linear electric machine is the dominant system in stelzer machine as shown in figure 1.

Several linear machine candidates exist including the PM machine, switched reluctance machine, and induction machine. Some research has been devoted to both the reluctance and induction machines, but their poor performance at low speeds has deemed them unsuitable for internal combustion engine [2]. As an alternative to these machines, this study develops an innovative linear transverse flux generator. The Transverse Flux Machines (TFMs) are a relatively new topology of electrical machines.

This study covers the analysis and design of electrically excited Linear Transverse Flux Machine (LTFM). It consists of two kinds of variable reluctance generator and magnets type; the former is Transverse Flux Electric excited (TFE), and the latter is Transverse Flux Permanent Magnet excited (TFPM). First of all, the liberal approximation such as Equivalent Magnetic Circuit (EMC) is made to obtain the idealized model and in order to keep the initial analysis simple excluding the saturation effects. It also suggests comparison on the result between 2-D and 3-D using Equivalent Magnetic Circuit Network (EMCN) method. As for the TFM, it is indispensable to analyze 3-D modeling due to the asymmetric structure in all the axis of *x*, *y*, and *z*-axis. At last, it is performed to verify the consilience of results between analytical calculation and numerical calculation by *3-D FLUX* software developed by *CEDRAT Group*.

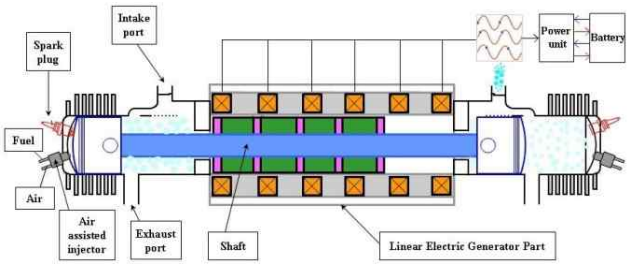

Fig. 1. Stelzer machine

2. Subjects of Investigation

The simplest feature of TFM is the similar to the configuration of switched reluctance machine. It has salient poles on both the stator and mover, but only one pair of

† Corresponding Author: Dept. of IT-Automotive Engineering, Gwangju University, Korea. (si.jeong@gwangju.ac.kr)
Received: October 31, 2017; Accepted: March 15, 2018

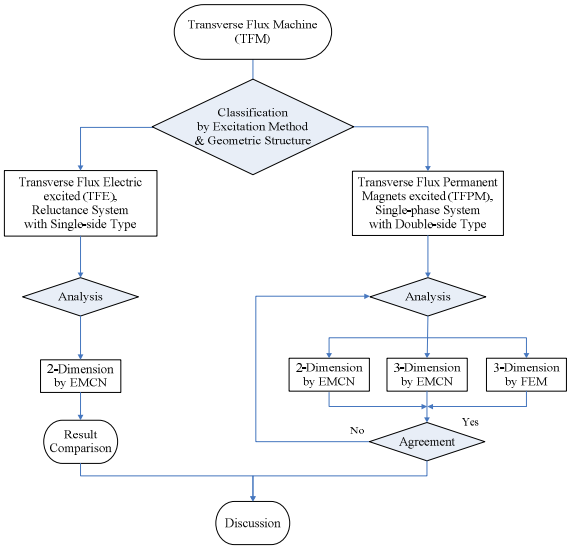

Fig. 2. Analysis process

member (stator or mover) carries excitation windings. In usual TFM's topology, the stator core is salient and the mover can be built up with or without salient poles. The mover is usually provided with magnets which are magnetized perpendicularly or parallel to moving direction of the mover. By structural and number of phase classification, it deals with TFE of reluctance type with single-phase system as single-sided topology and TFPM with single-phase system as double-sided topology. The analytical calculation of 2-D and 3-D by EMCN method is evaluated in each topology. Finally, the analytical result of double-sided TFPM topology is compared to numerical result simulated by FLUX 3-D software for a review of the validity of the 3-D result. The analytical design procedure is summarized by the flow chart of figure 2.

2.1. Single-sided TFE

The TFE machine is a variable reluctance type and it has a simple modular construction. This structure has been chosen because of the possibility to implement the control strategy of the machine from a customarily single-phase power converter. In particular, single-sided machines are easier to manufacture and have better prospects for practical applications. Besides, this machine has the advantage that is lower cogging force. When supplying the coil of a module with the stator teeth and the unaligned mover teeth, the mover teeth will tend to align with the stator teeth. Hence, the mover will be displaced one step length into the desired direction.

In figure 3, the simplest variant with two modules is presented. The stator coil is surrounded by *U-shaped* soft iron parts arranged on the mover circumstance. In order to establish the magnetic circuit adequately, an additional return path may be provided optionally by *I-shaped* soft iron pieces between the active stator poles. This reduces the leakage flux of the mover which weakens the main flux

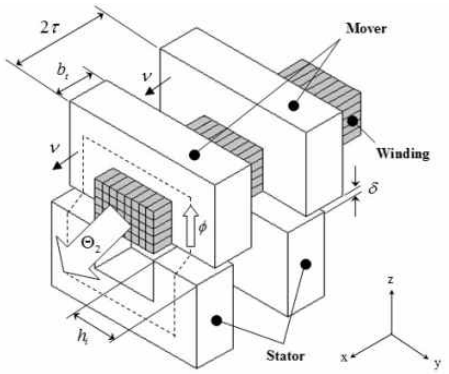

Fig. 3. Single-sided TFE machine

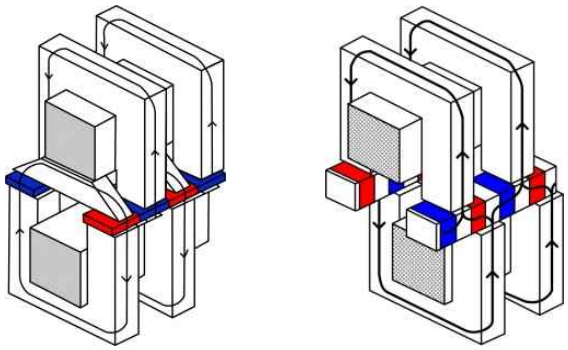

(a) Flat magnets mover (b) Inserted magnets mover

Fig. 4. Double-sided TFPM Machine

of the stator. All soft iron parts must be made of laminated steel in order to avoid important core losses due to the eddy-currents.

2.2. Double-sided TFPM

There are at least two double-sided topologies that can be used for building up the TFPM topologies with magnets on the mover. One consists of a mover with flat magnets inserted in between nonmagnetic material parts and two identical opposite stators. A variant of such a topology is shown in figure 4(a): it has U-shaped stator pole core and I-shaped return flux mover core. The other possible double-sides topology has a mover with concentrating flux poles and magnets inserted in between them, and magnetized in the direction of the mover movement. The variant of this double-sided TFPM topology shown in figure 4(b); it has two identical opposite stators with U-shaped pole core. In both cases presented for the double-sided TFPM, the stators are shifted with 180 electrical degrees.

3. Analytical Calculation of TFE

3.1. Thrust force in the direction of X-axis

If the magnetic flux density *B* is linearly related to the

magnetic field intensity H then the total energy stored in a steady magnetic field and the magnetic energy and co-energy become numerically the same. In other words, if a linear system is assumed, the superposition theory can be utilized to separately calculate the force acting on the system in the direction of x-, y-, and z-axis while other variables are held constant. Therefore, Eq. (1) shows the derivation using the co-energy equation.

$$W_{co}(\Theta, x) = \int_v \int_0^H B(H) \cdot dH\, dV$$
$$= \int_0^x \int_0^B B \frac{dB}{\mu_0} \delta \cdot h_i \cdot dx = \int_0^x \frac{B^2}{2 \cdot \mu_0} \delta \cdot h_i \cdot dx = \frac{B^2}{2 \cdot \mu_0} \delta \cdot h_i \cdot x$$
$$= \frac{B^2}{2 \cdot \mu_0} \delta \cdot h_i \cdot x = \frac{\mu_0^2 \cdot \Theta^2}{\delta^2} \cdot \frac{1}{2 \cdot \mu_0} \delta \cdot h_i \cdot x = \frac{\mu_0 \cdot \Theta^2}{2 \cdot \delta} h_i \cdot x \quad (1)$$

where, $dH = \frac{dB}{\mu_0}$, $dV = \delta \cdot h_i \cdot dx$, $B = \frac{\Theta \cdot \mu_0}{\delta}$

Using the derived co-energy Eq. (1), the force in the direction of x-axis can be obtained as in Eq. (2).

$$F_x(\Theta, x) = \frac{dW_{co}}{dx} = \frac{\mu_0 \cdot \Theta^2}{2 \cdot \delta} \cdot h_i \quad (2)$$

Where, Θ indicates MMF, while F_x indicates mechanical force.

Eq. (2) indicates that the force in the direction of x-axis is independent of position variable x. However, it should be noted that the equation only shows the behavior while position x is from 0 to τ. While the position is from τ to 2τ, the force is equal in magnitude and opposite in sign, since the teeth of the mover interact with the nearest teeth of stator, and the attraction causes opposite force while the position is from τ to 2τ. Therefore, in order to move the machine in positive direction, the current should be only applied during $0 < x < \tau$, and switched off during $\tau < x < 2\tau$. Fig. 5 illustrates the force in the direction of x-axis while a constant current is applied during $0 < x < \tau$, and zero current during $\tau < x < 2\tau$.

From the figure 5, the average force is a half of the force in Eq. (2). Therefore, the average force can be expressed as

$$F_{x\_mean} = \frac{F_x}{2} = \frac{\mu_0 \cdot \Theta^2}{4 \cdot \delta} \cdot h_i \ [N] \quad (3)$$

Also thrust force per air-gap, F_{ax}, can be expressed as

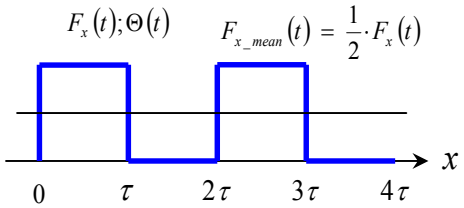

Fig. 5. Thrust Force in the Direction of X-axis

$$F_{ax} = \frac{F_{x\_mean}}{A_\delta} = \frac{F_{x\_mean}}{2 \cdot \tau \cdot h_i} = \frac{\mu_0}{8 \cdot \delta \cdot \tau} \cdot \Theta^2 \ [\frac{N}{m^2}] \quad (4)$$

Here, the A_δ is defined as the area covered by an air-gap during one period $2 \cdot \tau \cdot h_i$.

3.2. Lateral force in the direction of Y-axis

The lateral force in the direction of y-axis can be derived by Eq. (5); it shows the derivation using co-energy equation.

$$W_{co}(\Theta, h_i) = \int_v \int_0^H B(H) \cdot dH dV$$
$$= \int_0^{h_i} \int_0^B B \frac{dB}{\mu_0} \delta \cdot x \cdot dh_i = \int_0^{h_i} \frac{B^2}{2 \cdot \mu_0} \delta \cdot x \cdot dh_i = \frac{B^2}{2 \cdot \mu_0} \delta \cdot h_i \cdot x$$
$$= \frac{B^2}{2 \cdot \mu_0} \delta \cdot h_i \cdot x = \frac{\mu_0^2 \cdot \Theta^2}{\delta^2} \cdot \frac{1}{2 \cdot \mu_0} \delta \cdot h_i \cdot x = \frac{\mu_0 \cdot \Theta^2}{2 \cdot \delta} h_i \cdot x \quad (5)$$

where, $dH = \frac{dB}{\mu_0}$, $dV = \delta \cdot x \cdot dh_i$, $B = \frac{\Theta \cdot \mu_0}{\delta}$

This yields the identical result as Eq. (1). By taking derivative with respect to h_i yields the lateral force.

$$F_y(\Theta, h_i) = \frac{dW_{co}}{dh_i} = \frac{\mu_0 \cdot \Theta^2}{2 \cdot \delta} \cdot x \quad (6)$$

3.3. Attractive force in the direction of Z-axis

The flux in the air-gap not only generates force in the direction of x-axis and y-axis, but also causes the force in the direction of z-axis, which can be referred as attractive / normal force. This force acts on to minimize the air-gap δ, and the identical method shown in previous two paragraphs can be used. Eqs. (7) and (8) derive the co-energy and the force with respect to the direction of z-axis.

$$W_{co}(\Theta, \delta) = \frac{\mu_0 \cdot \Theta^2}{2 \cdot \delta} \cdot h_i \cdot x \quad (7)$$

$$F_z(\Theta, \delta) = \frac{dW_{co}}{d\delta} = -\frac{\mu_0 \cdot \Theta^2}{2 \cdot \delta^2} \cdot x \cdot h_i \quad (8)$$

Here, Eq. (8) derives the force generated by single air-gap. Since there are two air-gaps and the number of cores (N_{core}) per phase, rearranging Eq. (8) yields Eq. (9).

$$F_{z-phase} = \frac{\mu_0 \cdot \Theta^2}{2 \cdot \delta^2} \cdot x \cdot h_i \times 2 \times N_{core} = -N_{core} \cdot \frac{\mu_0 \cdot \Theta^2}{\delta^2} \cdot x \cdot h_i \quad (9)$$

As it can be seen from the Eq. (9), the attractive force is proportional to the inverse square of air-gap length; therefore, the air-gap length and its relation to attractive

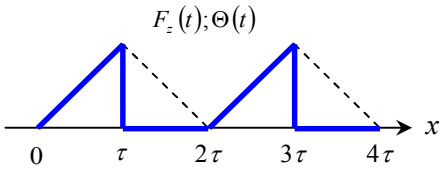

Fig. 6. Force in the Direction of *Z*-axis

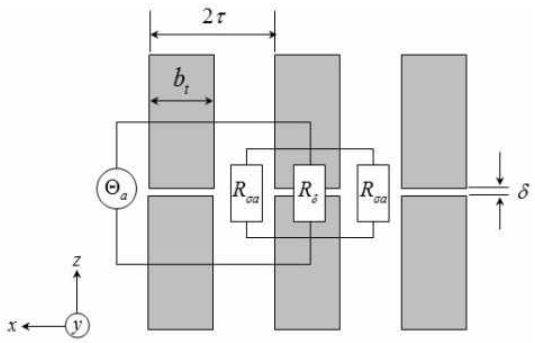

Fig. 7. Maximum Magnetic Energy in TFE (2-D)

force must be considered carefully during design. Another notable characteristic is that the attractive force is the function of x. Assuming that δ and h_i holds at constant values, the attractive force changes as linear motion travels in the direction of x-axis.

Fig. 6 illustrates the force characteristic in the direction of z-axis, as a function of position and MMF. During its operation, the current is only applied during $0<x<\tau$, and removed while $\tau<x<2\tau$, as it was explained in paragraph 3.1, and the generated force is shown with thick block line. In contrast, the dotted line shows the amount force if the current is constant for all time. The maximum attractive force occurs when the teeth of stator and the mover is aligned, which is equivalent to $x=\tau$. The minimum attractive force is zero, which occurs when the teeth are totally unaligned, which is equivalent to $x=0$.

3.4. Two-dimension EMC

In an electric-excited TFE of reluctance type, the average force can be similarly determined as having the above-mentioned energy method.

Fig. 7 shows the arrangement of the relations of the most important dimensions for the position of "tooth" against "tooth" for conformity and the EMC. The proposed EMC in TFE topology consists of two main parts, i.e., air-gap and leakage reluctance which also exist in the air region network.

$$\Theta_a = N_c \cdot I \tag{10}$$

$$R_\delta = \frac{\delta}{\mu_0 \cdot h_i \cdot b_t} \tag{11}$$

$$R_{\sigma a} = \frac{1}{\mu_0} \cdot \frac{\pi}{1} \cdot \frac{1}{h_i \cdot \ln\left(\frac{b_t}{\delta}\right)} \tag{12}$$

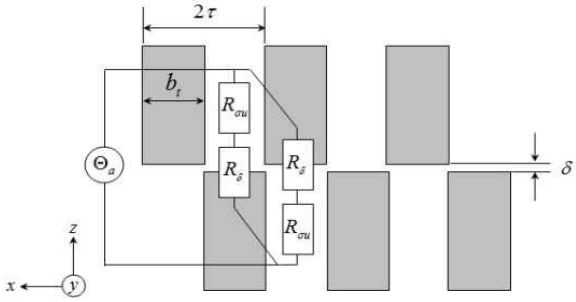

Fig. 8. Minimum Magnetic Energy in TFE (2-D)

Where, Θ_a, R_δ and $R_{\sigma a}$ are represent MMF, reluctance in air-gap and leakage reluctance in nonmagnetic material parts, respectively.

The configuration for the position of "tooth" against "slot" is shown in figure 8. Also, it is expressed as an EMC in that position. From above figure, the values of these reluctances can be calculated by applying *Ampere's* and *Kirchhoff's Law*. The leakage reluctance value under unaligned-position is given by

$$R_{\sigma u} = \frac{1}{\mu_0} \cdot \frac{2\tau - b_t}{h_i \cdot b_t} + \frac{1}{\mu_0} \cdot \frac{\pi}{2 \cdot h_i} \cdot \frac{1}{h_i \cdot \ln\left(\frac{b_t}{2 \cdot \tau - b_t}\right)} \tag{13}$$

By the EMC, it can be the difference of co-energy from the two positions and is calculated as follows

$$\Delta W_m = \Delta W_m \big|_{x=0} - \Delta W_m \big|_{x=r} = \Theta_a^2 \left[\frac{2R_\delta + R_{\sigma a}}{R_\delta \cdot R_{\sigma a}} - \frac{2}{R_\delta + R_{\sigma u}} \right] \tag{14}$$

Hence, the average force and force-density using the magnetic energy is achieved by Eq. (15) and (16), respectively. By calculating the force density, it is caused by the fact that the force in TFE machine is formed by one pole pitch during the movement.

$$F_{ave} = \frac{\Delta W_m}{\tau} \tag{15}$$

$$F_{den} = \frac{F_{ave}}{2\tau \cdot h_i} \tag{16}$$

4. Analytical Calculation of TFPM

4.1. Two-dimension EMC

The most common approach for force calculation by EMC method is based on analytical implementations of the virtual work method using spatial derivatives of air-gap reluctances [3~5], discrete evaluation of energies at two positions [6, 7], or electrical-equivalent circuit formulas based on flux linkages and currents [8].

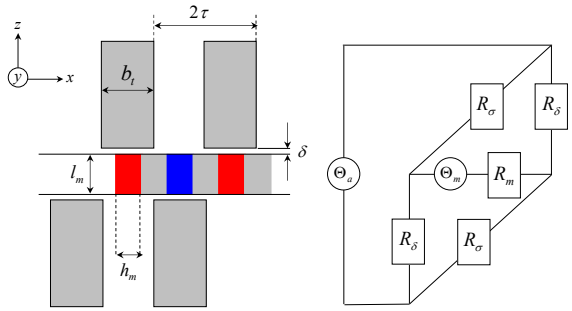

Fig. 9. EMC in TFPM (2-D)

Fig. 9 shows the arrangement of a TFPM machine which is magnetized into *x*-axis direction as a version of rectangular coordinates including the corresponding EMC sketch. The EMC shown in the configuration can be calculated using the following formulas. The MMF and reluctance in air-gap in double-sided topology are

$$\Theta_m = \frac{B_{rem} \cdot h_m}{\mu_0 \cdot \mu_r} \tag{17}$$

$$R_\delta = \frac{2 \cdot \delta}{\mu_0 \cdot h_i \cdot b_t} \tag{18}$$

$$R_m = \frac{1}{\mu_0} \cdot \frac{1}{h_i \cdot l_m} \cdot \frac{h_m}{\mu_r} \tag{19}$$

$$R_\sigma = \frac{1}{\mu_0} \cdot \frac{\tau - b_t + h_m}{h_i \cdot (\tau - h_m)} + \frac{1}{\mu_0} \cdot \frac{\pi}{2 \cdot h_i} \cdot \frac{1}{\ln\left(\frac{\tau - h_m}{\delta}\right)} \tag{20}$$

As given the Eq. (19) and (20), each of them represents reluctances in magnet and leakage in nonmagnetic material parts. Correspond to the EMC is calculated as the flux in each branch of the stator and mover to

$$\varphi_{a\delta} = \frac{\Theta_a \cdot (R_\sigma + R_m)}{2 \cdot R_\delta \cdot R_\sigma + (R_\sigma + R_\delta) \cdot R_m} \tag{21}$$

$$\varphi_{a\sigma} = \frac{\Theta_a \cdot (R_\delta + R_m)}{2 \cdot R_\delta \cdot R_\sigma + (R_\sigma + R_\delta) \cdot R_m} \tag{22}$$

$$\varphi_{m\delta} = \frac{\Theta_m \cdot R_\sigma}{2 \cdot R_\delta \cdot R_\sigma + (R_\sigma + R_\delta) \cdot R_m} \tag{23}$$

$$\varphi_{m\sigma} = \frac{\Theta_m \cdot R_\delta}{2 \cdot R_\delta \cdot R_\sigma + (R_\sigma + R_\delta) \cdot R_m} \tag{24}$$

The difference of the co-energy of the two positions for a pole element is

$$\begin{aligned} \Delta W_m &= \Delta W_m \big|_{x=0} - \Delta W_m \big|_{x=r} \\ &= [2(\varphi_{a\delta} + \varphi_{m\delta})^2 R_\delta + 2(\varphi_{a\sigma} - \varphi_{m\sigma})^2 R_\sigma \\ &\quad + (\varphi_{a\delta} - \varphi_{a\sigma} + \varphi_{m\delta} + \varphi_{m\sigma})^2 R_m] \\ &\quad - [2(\varphi_{a\delta} - \varphi_{m\delta})^2 R_\delta + 2(\varphi_{a\sigma} + \varphi_{m\sigma})^2 R_\sigma \\ &\quad + (\varphi_{a\delta} - \varphi_{a\sigma} - \varphi_{m\delta} - \varphi_{m\sigma})^2 R_m] \end{aligned} \tag{25}$$

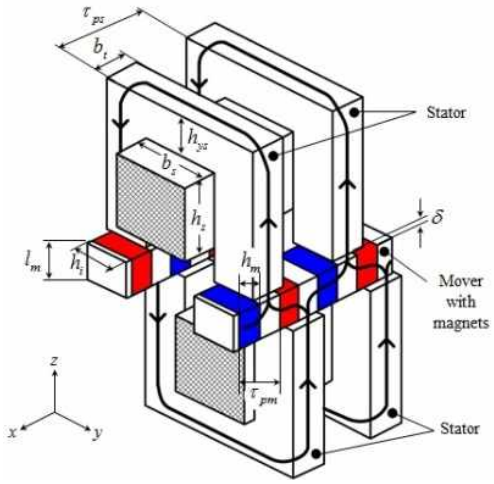

Fig. 10. TFPM Machine

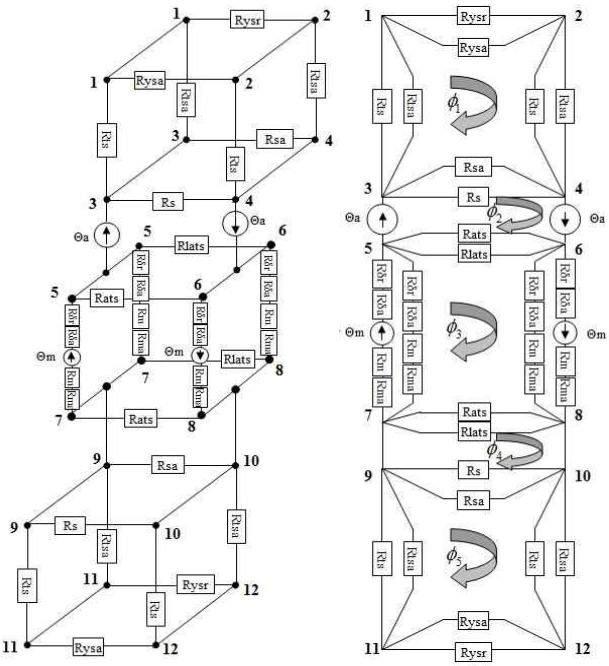

(a) 3-D View (b) 2-D Transformation

Fig. 11. Maximum Magnetic Energy in TFPM

The resulting average force and force density is calculated using the following equations.

$$F_{ave} = \frac{\Delta W_m}{\tau} \tag{26}$$

$$F_{den} = \frac{F_{ave}}{2\tau \cdot h_i} \tag{27}$$

4.2. Three-Dimension EMCN

The 3-D EMC is proposed to improve analytical modeling by taking into consideration the pole-to-pole flux

leakage. Due to the complex geometry of TFPM, there is no symmetry considering 2-D axis. So, the calculation of force and force density using magnetic energy has also been carried out based on the 3-D EMCN.

Fig. 10 presents the 3-D configuration of the TFPM which was selected as a more effective model by concentrating magnetic flux from the figure 4(b) The 3-D analysis is considered by dividing two positions (maximum and minimum magnetic energy) in the same way like 2-D analysis. For the calculations, the reluctances of the U-shaped core constituting the stator of the TFPM machine with the basic topology are described.

4.2.1. Aligned-position

In aligned position, the EMC for one pole element is expressed in figure 11; at first, it represents 3-D configuration and then indicates 2-D sketch for the sake of convenient calculation. The reluctances are calculated by mathematical expression as in the following. The R_{ysr} and R_{ysa} indicate the reluctance in the stator back-iron and in the air region between stacks, respectively.

$$R_{ysr} = \frac{b_t}{\mu_0 \mu_{fe} h_{ys} (b_s + 2h_i)} \tag{28}$$

for reluctance of axial direction in the stator back-iron

$$R_{ysa} = \frac{\tau_{ps} - b_t}{\mu_0 h_{ys} h_i} \tag{29}$$

for reluctance of axial direction between stacks in the air

The R_{ts} and R_{tsa} represent the reluctance of *z*-axis and axial direction in the stator teeth, respectively.

$$R_{ts} = \frac{1}{\mu_0 \mu_{fe} h_i b_t} \cdot \left(h_s + \frac{h_{ys}}{2} \right) \tag{30}$$

$$R_{tsa} = \frac{b_t}{\mu_0 \mu_{fe} h_i \left(h_s + \frac{h_{ys}}{2} \right)} \tag{31}$$

The R_s and R_{sa} show the leakage reluctance of *y*-axis and axial direction in slot, respectively.

$$R_s = \frac{b_s}{\mu_0 h_s b_t} \tag{32}$$

for leakage reluctance of *y*-axis direction in slot

$$R_{sa} = \frac{\tau_{ps}}{\mu_0 h_s b_s} \tag{33}$$

for leakage reluctance of axial direction in slot

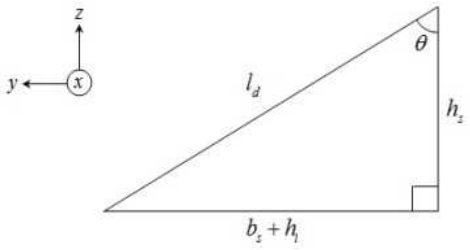

Fig. 12. Configuration for R_{ats} and R_{lats}

The $R_{\delta r}$ and $R_{\delta a}$ express the reluctance of *z*-axis and axial direction in air-gap, respectively.

$$R_{\delta r} = \frac{\delta}{\mu_0 h_i h_m} \tag{34}$$

for reluctance of *z*-axis direction in air-gap

$$R_{\delta a} = \frac{\tau_{pm} - h_m}{\mu_0 h_i l_m} \tag{35}$$

for reluctance of axial direction in air-gap

The R_{ats} and R_{lats} are the reluctance caused by *y*-axis and leakage of axial direction in air region between stator stacks, respectively.

They can be obtained conveniently by the formulas and using the figure 12 expressed with *y*- and *z*-axis 2-D coordinate.

$$\theta = \tan^{-1}\left(\frac{b_s + h_i}{h_s} \right) \tag{36}$$

$$l_d = \sqrt{(b_s + h_i)^2 + h_s^2} \tag{37}$$

$$R_{ats} = \frac{\theta \cdot l_d}{\mu_0 h_i b_t} \tag{38}$$

$$R_{lats} = \frac{\theta \cdot l_d}{\mu_0 h_i (\tau_{ps} - b_t)} \tag{39}$$

The R_m and R_{ma} signifies the reluctance of axial and *y*-axis direction in magnet, respectively.

$$R_m = \frac{h_m}{\mu_0 h_i l_m} \tag{40}$$

$$R_{ma} = \frac{h_m}{\mu_0 h_i (\tau_{pm} - l_m)}, \tag{41}$$

In aligned position, the matrix equation for the flux can be expressed as Eq. (42) by figure 11(b) converted from 3-D organization.

$$\begin{vmatrix}\varphi_1\\ \varphi_2\\ \varphi_3\\ \varphi_4\\ \varphi_5\end{vmatrix} = \begin{vmatrix} \frac{R_{ysr}\cdot R_{ysa}}{R_{ysr}+R_{ysa}}+2\cdot\left(\frac{R_{tsa}\cdot R_{ts}}{R_{tsa}+R_{ts}}\right)+\frac{R_{sa}\cdot R_s}{R_{sa}+R_s} & -\frac{R_{sa}\cdot R_s}{R_{sa}+R_s} & 0 & 0 & 0 \\ -\frac{R_{sa}\cdot R_s}{R_{sa}+R_s} & \frac{R_{sa}\cdot R_s}{R_{sa}+R_s}+\frac{R_{ats}\cdot R_{lats}}{R_{ats}+R_{lats}} & -\frac{R_{ats}\cdot R_{lats}}{R_{ats}+R_{lats}} & 0 & 0 \\ 0 & -\frac{R_{ats}\cdot R_{lats}}{R_{ats}+R_{lats}} & 2\cdot\left(\frac{R_{ats}\cdot R_{lats}}{R_{ats}+R_{lats}}\right)+2\cdot\left(\frac{R_{\delta a}+R_{\delta r}+R_m+R_{ma}}{2}\right) & -\frac{R_{ats}\cdot R_{lats}}{R_{ats}+R_{lats}} & 0 \\ 0 & 0 & -\frac{R_{ats}\cdot R_{lats}}{R_{ats}+R_{lats}} & \frac{R_{ats}\cdot R_{lats}}{R_{ats}+R_{lats}}+\frac{R_{sa}\cdot R_s}{R_{sa}+R_s} & -\frac{R_{sa}\cdot R_s}{R_{sa}+R_s} \\ 0 & 0 & 0 & -\frac{R_{sa}\cdot R_s}{R_{sa}+R_s} & -\frac{R_{sa}\cdot R_s}{R_{sa}+R_s}+2\cdot\left(\frac{R_{ts}\cdot R_{tsa}}{R_{ts}+R_{tsa}}\right)+\frac{R_{ysa}\cdot R_{ysr}}{R_{ysa}+R_{ysr}} \end{vmatrix}^{-1} \cdot \begin{vmatrix}0\\ 2\Theta_a\\ 2\Theta_m\\ 0\\ 0\end{vmatrix} \tag{42}$$

$$\begin{vmatrix}\varphi_6\\ \varphi_7\\ \varphi_8\\ \varphi_9\\ \varphi_{10}\end{vmatrix} = \begin{vmatrix} \frac{R_{ysr}\cdot R_{ysa}}{R_{ysr}+R_{ysa}}+2\cdot\left(\frac{R_{tsa}\cdot R_{ts}}{R_{tsa}+R_{ts}}\right)+\frac{R_{sa}\cdot R_s}{R_{sa}+R_s} & -\frac{R_{sa}\cdot R_s}{R_{sa}+R_s} & 0 & 0 & 0 \\ -\frac{R_{sa}\cdot R_s}{R_{sa}+R_s} & \frac{R_{sa}\cdot R_s}{R_{sa}+R_s}+\frac{R_{ats}\cdot R_{lats}}{R_{ats}+R_{lats}} & -\frac{R_{ats}\cdot R_{lats}}{R_{ats}+R_{lats}} & 0 & 0 \\ 0 & -\frac{R_{ats}\cdot R_{lats}}{R_{ats}+R_{lats}} & 2\cdot\left(\frac{R_{ats}\cdot R_{lats}}{R_{ats}+R_{lats}}\right)+2\cdot\left(R_{\delta a}+R_{\delta r}+R_m\right) & -\frac{R_{ats}\cdot R_{lats}}{R_{ats}+R_{lats}} & 0 \\ 0 & 0 & -\frac{R_{ats}\cdot R_{lats}}{R_{ats}+R_{lats}} & \frac{R_{ats}\cdot R_{lats}}{R_{ats}+R_{lats}}+\frac{R_{sa}\cdot R_s}{R_{sa}+R_s} & -\frac{R_{sa}\cdot R_s}{R_{sa}+R_s} \\ 0 & 0 & 0 & -\frac{R_{sa}\cdot R_s}{R_{sa}+R_s} & -\frac{R_{sa}\cdot R_s}{R_{sa}+R_s}+2\cdot\left(\frac{R_{ts}\cdot R_{tsa}}{R_{ts}+R_{tsa}}\right)+\frac{R_{ysa}\cdot R_{ysr}}{R_{ysa}+R_{ysr}} \end{vmatrix}^{-1} \cdot \begin{vmatrix}0\\ 2\Theta_a\\ 2\Theta_m\\ 0\\ 0\end{vmatrix} \tag{43}$$

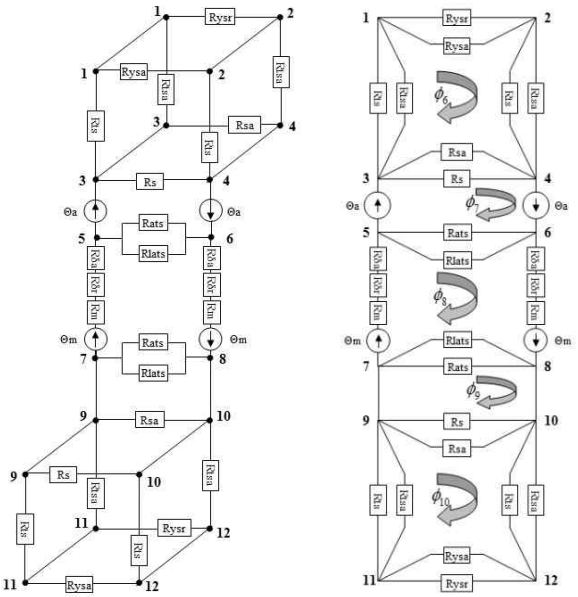

(a) 3-D View (b) 2-D transformation

Fig. 13. Minimum magnetic energy in TFPM

4.2.2. Unaligned-position

The calcultion for the flux matrix equation in unaligned position is achieved identically as the formula in aligned position.

In addition, the calculation of the average force and force density is same as 2-D EMC calculation method.

$$F_{ave} = \frac{W_m}{\tau_{pm}} \tag{44}$$

$$F_{den} = \frac{F_{ave}}{2\tau_{pm}\cdot h_i} \tag{45}$$

5. Comparison Results

In a prior study, the analytical model for the analysis of the TFPM was established. Based on the given mathematical model, analytical calculation using the magnetic energy and force characteristics was computed by a 2-D and 3-D EMCN method respectively. This performance roughly analyzed with the help of the developed analytical models. However, previous experience of the TFM showed that the analytical models cannot be relied to a great extent. Thus, it is required for 3-D FEM analysis, which is a kind of numerical calculation for verification of analytical calculation. At last, the results are compared to those obtained by 2-D and 3-D analytical models. Fig. 14 indicates the direction and degree of the magnetic flux by excited winding and magnets. Based on this simulation, the evaluation of the results will be performed with the

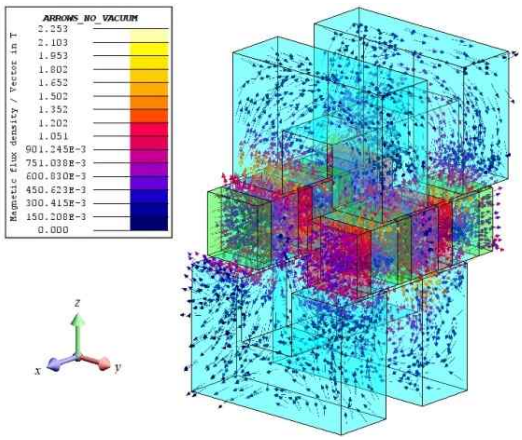

Fig. 14. The Investigated 3-D FEM of TFPM

Table 1. Estimation by EMC and FEM

-	TFPM		
	Analytical Calculation (EMCN)		Numerical calculation
	2-D	3-D	3-D FEM
Magnetic Energy [*J*]	0.08	0.081	0.074
Average Force [*N*]	8.89	8.959	8.216
Force Density [*N/mm²*]	49.4	49.77	45.64

analytical calculated results.

Generally, the serious loss in force is caused by high stator leakage flux. It can be become evident from 3-D FE analysis. A comparison between analytical calculation and 3-D FE analysis result by the magnetic energy, average force and force density is given for in table 1. The result by 3-D FEM is coincide with over 90 [%] in comparison previous analytical results by 2-D and 3-D EMCN.

6. Conclusion

In this study, two different kinds of TFM are discussed ; TFE and TFPM with single -phase system. In a correlation between two models, the former is considered as single-sided reluctance type, the latter is regarded as model that consists of double-sided stators with magnets in mover. The design process of these models takes advantage of the methods by 2-D and 3-D EMCN analysis. Finally, the analytical calculations by EMCN method are evaluated through 3-D FEM simulated result. As a result, the results of analytical estimation by EMCN are much satisfied with that of FE analysis by FLUX 3-D. However, this study was overlooked the leakage flux generated from *z*-axis direction between the upper and lower stator cores. To reduce the errors shown in the table 1, it needs more investigation of the leakage flux generated in the area above.

It will give elaborate information about the design rules and performance data of LTFM and in parallel tools for the calculation, simulation and design will be available.

Acknowledgements

This study was conducted by research funds from Gwangju University in 2018.

Reference

[1] Sung In Jeong, *Comparative Study of Linear Oscillating Generators*, Dissertation an der Technischen Universität Braunschweig, 2015.

[2] J. Vining, T.A. Lipo, G. Venkataramanan, *Design and Optimization of a Novel Hybrid Transverse / Longitudinal Flux, Wound-Field Linear Machine for Ocean Wave Energy Conversion*, 978-1-4244-2893-9/09/$25.00 ©2009 IEEE.

[3] S. A. Nasar, *Electromagnetic Energy Conversion Devices and Systems*.

[4] R. Qu and T. A. Lipo, "Analysis and modeling of air-gap and zigzag leakage fluxes in a surface-mounted permanent magnet machine," *IEEE Trans. Ind. Appl.*, vol. 40, no. 1, pp. 121-127, Jan./Feb. 2004.

[5] V. Ostović, *Dynamics of Saturated Electric Machines,* New York, Springer-Verlag, 1989.

[6] P. Sewell, K. J. Bradley, J. C. Clare, P. W. Wheeler, A. Ferrah, and R. Magill, "Efficient dynamic models for induction machines," *Intl. J. Numer. Model.*, vol. 12, pp. 449-464, 1999.

[7] H. Meshgin-Kelk, J. Milimonfared, and H. A. Toliyat, "A comprehensive method for the calculation of inductance coefficients of cage induction machines," *IEEE Trans. Energy Conversion*, vol. 18, pp. 187-193, Jun. 2003.

[8] J. Perho, "Reluctance network for analysing induction machines," *Acta Polytechnica Scandinavica, Electrical Engineering Series*, vol. 110, pp. 1-147, Dec. 2002.

Sung-In Jeong He received B.S. and M.S. degrees in Electrical Engineering from Dongguk and Hanyang University, South Korea, respectively. And then he was responsible for the development of electrical machine and its drive at Samsung Heavy Industry, Samsung Electronics, and Daewoo Electronics, in order. After he received Dr.-Ing. degree from Technical University Braunschweig, Germany. He was in the Daelim Motor, South Korea. Since March 2018, he has joined Gwangju University, where he is currently a Professor in the Division of IT-Automotive Engineering. His research and development field and interest included design, analysis and drive of electric machine for electric and smart personal motilities.